Astron. Astrophys. 334, 1028–1036 (1998)

ASTRONOMY AND ASTROPHYSICS

# Determination of the length of coronal loops from the decay of X-ray flares

## II. Stellar flares observed with ROSAT/PSPC

**F. Reale**[1] **and G. Micela**[2]

[1] Dipartimento di Scienze Fisiche e Astronomiche, Università di Palermo, Sezione di Astronomia, Piazza del Parlamento 1, I-90134 Palermo, Italy (reale@oapa.astropa.unipa.it)
[2] Osservatorio Astronomico, Piazza del Parlamento 1, I-90134 Palermo, Italy (micela@oapa.astropa.unipa.it)

Received 30 June 1997 / Accepted 27 February 1998

**Abstract.** We illustrate a procedure to estimate the length of stellar coronal loops from the decay of X-ray flares observed with ROSAT/PSPC. As we did in the first paper of this series for solar flares, we use extensive hydrodynamic modeling, and the synthesis of observable quantities from the model results, to obtain an expression for the loop length in terms of parameters readily derivable from spectrally-resolved X-ray light curves, such as those of ROSAT/PSPC. The length estimate takes into account the effect of possible sustained heating during the decay and is derived from a quantity measuring PSPC spectral shape variations (Spectral Shape Index, SSI), which is a temperature indicator, and from the global light curve. Self-consistency tests on models have shown that the loop length estimation should not suffer from systematic errors, and that its uncertainty ranges from $\sim$ 20% for $\sim$ 40000 counts in the flare observation to $\sim$ 70% for $\sim$ 1000 counts. The effect of interstellar absorption is discussed and the appropriate corrections derived. As test applications, we derive the loop length for two flares, one on the M star AD Leo and the other on the M star CN Leo.

**Key words:** stars: coronae – stars: flare

### 1. Introduction

The similar phenomenology of solar and stellar flares suggests that they share a common physical scenario. The gross features of many solar flares (e.g. light curves) can be described quite well in the hypothesis that they occur inside closed magnetic loops, whose geometry does not change during the flare. We may then imagine to extend this scenario to stellar flares, although on different scales and environmental conditions. Since, due to distance, flaring loops cannot be imaged on stars as it can be done on the Sun, one can consider using this solar-stellar connection to obtain information on the geometry and the size of the loops. In particular the dependence of the flare decay time on the characteristic cooling times of the confined plasma has been used in the past to infer the length of stellar flaring structures ( e.g. Haisch 1983, Reale et al. 1988, van den Oord et al. 1988). However, the presence of a significant sustained heating release during the decay can delay the plasma cooling, thus seriously affecting these estimates, and ultimately making them only upper limits. The problem of loop length estimation is further complicated by the wide band spectral response of typical extrasolar X-ray telescopes, such as ROSAT/PSPC. The observed light curve is the result of the concurrence and integration of many effects, both physical and instrumental, which make the correspondence between physical cooling times and light curve decay time non-trivial.

A previous paper (Reale et al. 1997, hereafter paper I) has shown how to obtain a reliable estimate of the flaring loop length from the analysis of the decay of X-ray flares, even taking into account the presence of significant heating during the decay.

The approach is based on extensive hydrodynamic modeling of decaying flaring loops, which has allowed the authors to propose and test a relationship between the decay time of the X-ray light curve and the slope of the trajectory in the density-temperature diagram. From this relationship, an expression of the loop length as a function of the decay time, of the slope and of the flare maximum temperature has been obtained. This expression yields the loop length directly from the flare data with no need to model the event in detail.

The testing ground for the method has been a set of solar flares well-observed and imaged with the Soft X-ray Telescope (SXT) on board the Yohkoh satellite. The moderate spectral resolution and high spatial/temporal resolution of Yohkoh/SXT allowed us, on the one hand, to infer the loop lengths from the analysis of the decay, and, on the other, to compare them consistently with the size of the structures measured directly on the SXT images.

Although the modeling is based on the assumption of compact flares occurring in single coronal loops, good estimates of the size of the flaring regions are obtained even when the geometry is not so simple (Paper I).

When we turn our attention to stellar flares, we have to take into account that these are generally more energetic and long-

*Send offprint requests to*: F. Reale

lasting than solar flares, thus suggesting larger structures and larger amounts of energy released (e.g. Haisch et al. 1991). The decay may be influenced by the flare occurrence in large structures, comparable to the local pressure scale height (Reale et al. 1993).

A generalized application may be made difficult both by the low data statistics and spectral resolution, and by the integration over the whole stellar disk and over long times compared to the time scale of the thermal variations of the flaring plasma. These features, intrinsic to stellar flare observations, cause large uncertainties in the determination of the flare temperature and emission measure, but also the impossibility to follow the flare decay down to low emission, due to the presence of the steady background coronal emission. A way to take care of this problem is to look for alternative model-independent tracers, which, although being without a straightforward physical meaning, are more efficient in detecting spectral variations during the decay, thus optimizing for the available statistics. In the following we show how we take best advantage of stellar PSPC data, replacing the temperature with a Spectral Shape Index (SSI) derived from a principal component analysis applied to model instrument spectra (see Sciortino et al. 1996, for preliminary results).

Finally, it should be considered that flares often occur on young stars of star-forming regions, which are embedded in large and dense clouds which can absorb significant fractions of the emitted radiation, and modify the source spectra.

The extension to stellar flares has therefore required us to tackle properly the following topics: a) the extension to loop structures comparable to, or larger than, the local pressure scale height; b) a particular care in extracting the maximum of the information from the data; c) the effect of interstellar absorption.

Although the method is general and generalizable to all X-ray instruments with spectral and temporal resolution, here we will describe the method for the ROSAT/PSPC, which has collected a large amount of stellar flare observations (Sect. 2). The application to two specific flares, one observed on the star AD Leo and the other on CN Leo, is described in Sect. 3 and our conclusions are in Sect. 4.

## 2. Length estimation

### *2.1. Modeling*

In Paper I a rule has been devised to derive the length of flaring coronal loops, observed on the Sun by the Yohkoh SXT, from the analysis of the light curve decay and of the decay path in the $\overline{n}$-T diagram, where $\overline{n}$ is the square root of the emission measure $EM$. By means of extensive numerical hydrodynamic loop modeling (Betta et al. 1997) of the flare decay phase, a relationship has been found between the slope $\zeta$ in the $\overline{n}$-T diagram and the light curve decay time $\tau_{LC}$, normalized to the spontaneous loop decay time $\tau_{th}$ (Serio et al. 1991):

$$\tau_{th} = \alpha L/\sqrt{T_{max}} \qquad (1)$$

where $\tau_{th}$ is in seconds, $\alpha = 3.7\,10^{-4}\,\mathrm{s\,cm^{-1}\,K^{1/2}}$, $L$ the loop half-length (cm) and $T_{max}$ the flare maximum temperature (K), generally located at the loop apex. This has allowed us to obtain a relationship giving $L$, depending only on $\tau_{LC}$, $\zeta$ and $T_{max}$, and taking into account the effect of prolonged heating during the decay.

In spite of the generality of the approach – the fundamental requirement is to have temperature diagnostics – the parameters of the formula for $L$ depend non-trivially on the synthesized light curve and on the determination of the temperature and emission measure. Therefore, although we expect a general similarity when we consider other X-ray telescopes, such as ROSAT/PSPC, the numerical values of the parameters are to be adjusted to the instrumental spectral response.

In order to obtain an equivalent expression for the flaring loop length for ROSAT/PSPC observations, here we will follow the same step-by-step derivation done for solar observations. The ROSAT/PSPC has imaging capabilities and moderate spectral resolution with $\Delta E/E = 0.43(E/0.93)^{-0.5}$ FWHM, in the energy band 0.1-2.5 keV. We have divided this band into 34 channels.

We will at first neglect the problem of the limited count statistics, by assuming infinite data statistics, and also neglect the effect of interstellar absorption when synthesizing the loop spectra from model results, i.e. we assume $N_H \sim 0$.

As described in Paper I, we model the flare decay by letting the loop plasma evolve from flare maximum conditions, and switching off, either abruptly or gradually with an exponential decay, the heating which brought the loop to flaring conditions. In order to generalize our description, we will consider both the same model loops with solar gravity as in Paper I, and other models of decaying loops on stars with different superficial gravity and radius. Also for the additional loops several values of the heating decay time have been considered.

One basic point of our approach is to analyze the hydrodynamic model results as we would analyze real data. We do this by synthesizing ROSAT/PSPC spectra $\mathcal{L}_i$ from the density and temperature distributions along the loop sampled during the flare decay which we obtain from the modeling:

$$\mathcal{L}_i(t) = \mathcal{A}\int_0^{s_{max}} n^2(s,t)G_i(T(s,t))ds \qquad i = 1,34 \qquad (2)$$

where $\mathcal{A}$ is the loop cross-sectional area, which is assumed to be constant along the loop, $n(s,t)$, $T(s,t)$ are the plasma number density and temperature along the loop, $G_i(T)$ is the plasma emissivity folded through the instrumental response per unit emission measure in the $i$-th PSPC channel, $s$ is the field line coordinate along the loop and $t$ is the time. These spectra are the analogues of real PSPC spectra, from which the background and the steady-state stellar emission spectra have been subtracted. By summing the luminosity in all relevant channels we obtain the global light curve.

In analogy to the procedure followed for Yohkoh/SXT, we should then derive the path in the density-temperature diagram. In order to do this, we may fit the spectra with one-temperature model spectra obtained folding Raymond-Smith (1977) isothermal plasma spectra with the PSPC energy response, as routinely

done when analyzing ROSAT/PSPC stellar observations. However, it is well established that this kind of simplified 1-T models is often not appropriate to describe the stellar loop emission (Ciaravella et al. 1997), and the temperature value obtained from fitting real data may have no meaning for relatively high $\chi^2$'s, or may be easily affected by large indeterminations.

### *2.2. Spectral shape index*

For a more appropriate analysis of flares observed with ROSAT/PSPC, we have decided to consider a model-independent temperature indicator, obtained as a linear combination of PSPC channels and optimized by means of the Principal Component Analysis (PCA, e.g. Murtagh & Heck 1987). This indicator, which we will call "Spectral Shape Index" (SSI), has the advantage to be directly obtained from the data requiring no spectral fit procedure.

An example of the application of PCA to low resolution X-ray spectra can be found in Collura et al. (1995), where the PCA is used to determine the linear combinations of spectral channels (colors) that maximize the spread observed in spectra of X-ray sources detected with the *Einstein*/IPC (Giacconi et al. 1979).

To determine the principal components we have generated and instrument-filtered a set of noiseless spectra from hydrostatic loop models (Serio et al. 1981). We are confident of the reliability of the use of hydrostatic loops because, due to the relatively negligible role of plasma dynamics during the flare decay, they are a good approximation of the instantaneous flaring loop conditions. Our set of loops consists of 105 loops with half length $L = 0.3, 1, 3, 10, 30 \times 10^9$ cm and temperature between $10^6$ and $10^8$ K. The explored parameter space includes loops with length both smaller and larger than the pressure scale height.

The first step of the analysis is the normalization of the spectra with respect to the total counts. This step is necessary because we want to characterize just the shape of the spectra and not their intensity. We will consider channels 6-34, which have turned out to be the most appropriate to analyze flares. The normalization reduces the number of degrees of freedom to 28, so we use the channels from 6 to 33 (channel 34 can be obtained as a linear combination of the other channels). At this point our data set consists of a sample of 105 points in the 28-dimension space defined by the 6-33 channels. We then scale the counts in each channel, i.e. the variables are measured as deviations from the mean of each channel in units of standard deviation. With this choice each channel has the same weight in the component definition. In practice each new variable $V$ is computed from the original channel $C$ as:

$$V_{i,n} = \frac{C_{i,n}/\sum_{i=6}^{34} C_{i,n} - < C_i >}{\sigma_{C_i}} \quad (3)$$

where $V_{i,n}$ is the new $i$-th variable for the spectrum $n$, $C_{i,n}$ the original $i$-th channel of the $n$-th spectrum, $< C_i >$ and $\sigma_{C_i}$ are the mean value and the standard deviation of the $i$-th channel of all spectra, respectively. The values of $< C_i >$ and $\sigma_{C_i}$ for our data set are reported in Table 1.

**Table 1.** Mean values, standard deviations for scaling the observed spectra, and weights of ROSAT/PSPC channels that determine the first component.

| C | $< C >$ | $\sigma_C$ | W |
|---|---|---|---|
| 6 | 0.18571 | 0.10731 | -0.21 |
| 7 | 0.14077 | 0.07299 | -0.21 |
| 8 | 0.09305 | 0.04382 | -0.22 |
| 9 | 0.06424 | 0.02694 | -0.21 |
| 10 | 0.03169 | 0.01063 | -0.20 |
| 11 | 0.01868 | 0.00434 | -0.11 |
| 12 | 0.01592 | 0.00448 | 0.07 |
| 13 | 0.02170 | 0.00842 | 0.13 |
| 14 | 0.02822 | 0.01297 | 0.15 |
| 15 | 0.03550 | 0.01820 | 0.16 |
| 16 | 0.04802 | 0.02679 | 0.17 |
| 17 | 0.05097 | 0.03019 | 0.18 |
| 18 | 0.04946 | 0.03042 | 0.19 |
| 19 | 0.05037 | 0.03197 | 0.20 |
| 20 | 0.04077 | 0.02694 | 0.21 |
| 21 | 0.03103 | 0.02169 | 0.22 |
| 22 | 0.02316 | 0.01735 | 0.22 |
| 23 | 0.01901 | 0.01538 | 0.22 |
| 24 | 0.01369 | 0.01195 | 0.21 |
| 25 | 0.01006 | 0.00936 | 0.20 |
| 26 | 0.00823 | 0.00808 | 0.20 |
| 27 | 0.00599 | 0.00614 | 0.19 |
| 28 | 0.00436 | 0.00461 | 0.19 |
| 29 | 0.00344 | 0.00369 | 0.19 |
| 30 | 0.00239 | 0.00259 | 0.19 |
| 31 | 0.00159 | 0.00174 | 0.19 |
| 32 | 0.00100 | 0.00111 | 0.19 |
| 33 | 0.00064 | 0.00072 | 0.18 |

The PCA has been applied to the resulting 105 normalized and scaled spectra from channels 6 to 33 (0.2 - 2.4) keV. The percentage of the variance explained by the first component is $\sim$ 72% of the entire variance, and increases to 92% if we consider the first two components. The weights of the channels that determine the first component, our SSI, are reported in the fourth column of Table 1. The linear combination which defines the SSI of the $n$-th spectrum is then:

$$SSI_n = \sum_i W_i V_{i,n} \quad (4)$$

The SSI measures the hardness of the spectrum, and we expect that it should be related to some representative temperature of the loops generating the components. Fig. 1 shows the relationship between the first component and the maximum temperature of loops with length much shorter than the local pressure scale height, and between the first component and the temperature at the pressure scale height for longer loops. Since flares occur also in young stars in star forming regions or open clusters, we have explored how the relationship between the SSI and the temperature changes with the presence of interstellar

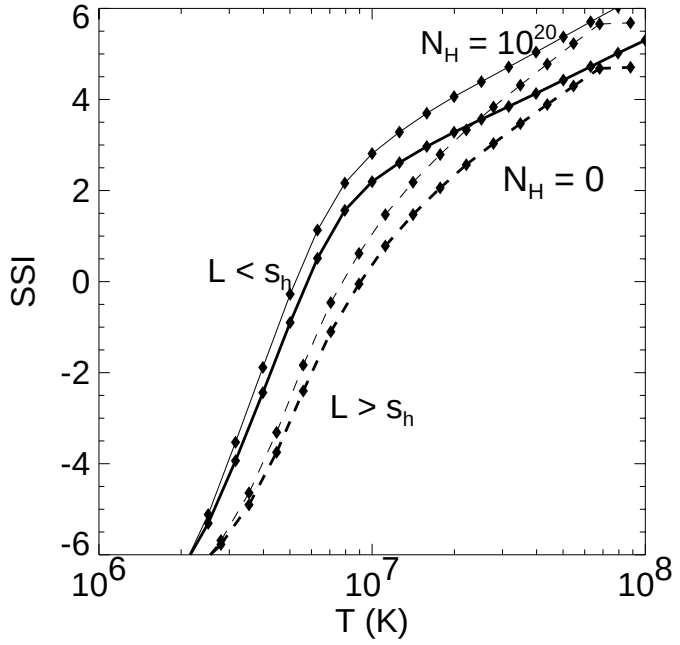


**Fig. 1.** Spectral Shape Index (SSI) vs. maximum temperature of hydrostatic loop models (*data points*) (Serio et al. 1981), with solar gravity and half-length smaller ($3 \times 10^9$ cm, *solid lines*) and longer (*dashed lines*) than the local pressure scale height ($s_h$). For the latter ones the temperature is taken *at* the pressure scale height. The SSI values are computed for no absorption (*thick lines*) and for $\log N_H = 20$ (*thin lines*).

absorption. Fig. 1 also shows the same curves for loops observed through a hydrogen column of $\log N_H = 20$.

We have ascertained that a hardness ratio, defined as a simple linear combination of the PSPC channels, with equal weights, is not as appropriate as a temperature tracer for flares, since it is not a monotonic function of temperature in the temperature range of interest.

### *2.3. Length formula*

As outlined in Sect. 1 and 2.1, our diagnostical method is based on the analysis of the decay of the light curve and of the path in a density-temperature diagram.

In our analysis of ROSAT/PSPC flare data, the temperature will be replaced by the SSI defined in Sect. 2.2 (Eq. 4). Rather than the density we will consider *the square root of the count rate* (CR2), as integrated in the selected 28 channels. The count rate in fact scales well with the emission measure (see Eq. 2), provided that the instrumental response function $G_i(T)$ has a smooth dependence on temperature in the range of interest, which is the case for ROSAT/PSPC. Therefore we will identify the trajectory of the flare decay in a CR2 - SSI diagram.

Fig. 2 shows an example of PSPC light curve and trajectory in the CR2-SSI diagram, for the decay of a model solar flaring loop with half-length $L = 2 \times 10^9$ cm, maximum temperature $T_{max} = 2 \times 10^7$ K, and no heating during the decay ($\tau_H = 0$). Notice how the shape of the light curve and its decay time, the latter being significantly longer than that obtained for Yohkoh/SXT (see Fig. 1 in Paper I), are influenced by the folding of the whole loop plasma emission with the wide band energy response of the PSPC. We define the light curve decay time $\tau_{LC}$ as the time taken by the count rate to decrease by $1/e$ from the maximum value.

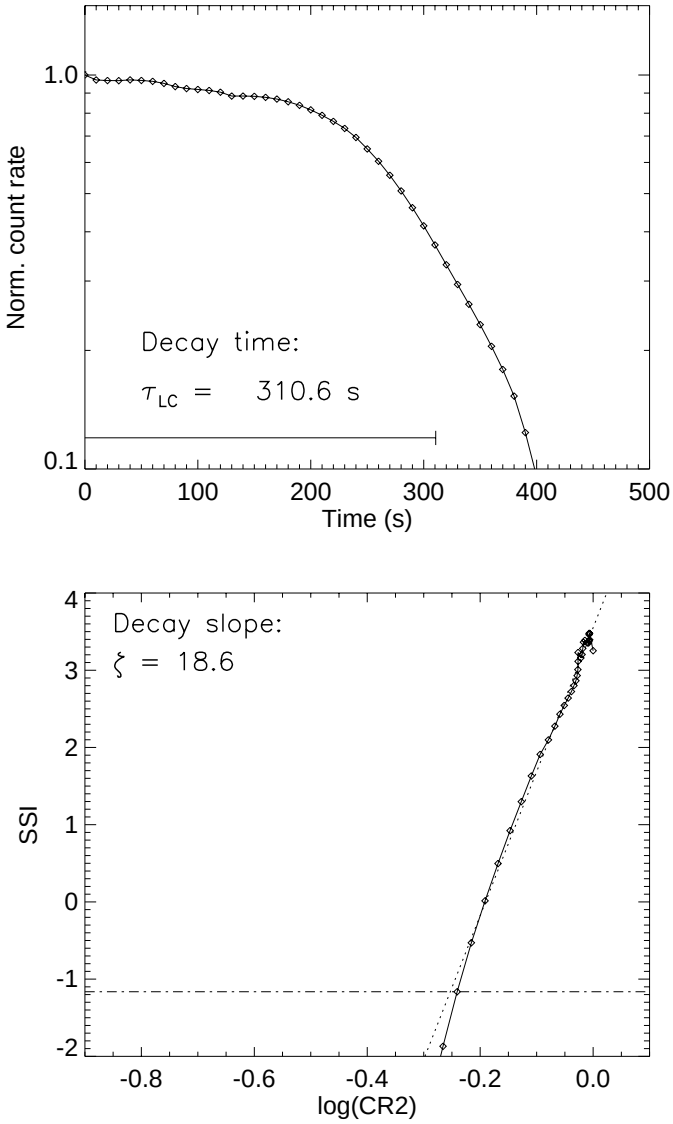


**Fig. 2.** Synthesized ROSAT/PSPC light curve (*upper panel*) and trajectory in the CR2-SSI diagram (*lower panel*) of the decay of a model flaring loop with semilength $L = 2 \times 10^9$ cm, maximum temperature $T_{max} = 2 \times 10^7$ K, and no heating during the decay ($\tau_H = 0$). In the CR2-SSI diagram, the best fit (*dashed*) line with slope ($\zeta$) and the lowest SSI used for the linear regression (*dashed-dotted line*) are shown.

The CR2 - SSI diagram (Fig. 2) shows a well defined path. The best-fit line, and its slope $\zeta$, are obtained with a linear regression from the light curve maximum to 1/3 of the maximum count rate.

Fig. 3 shows the light curve decay time, as normalized to the spontaneous thermodynamic loop decay time, $\tau_{LC}/\tau_{th}$, vs.

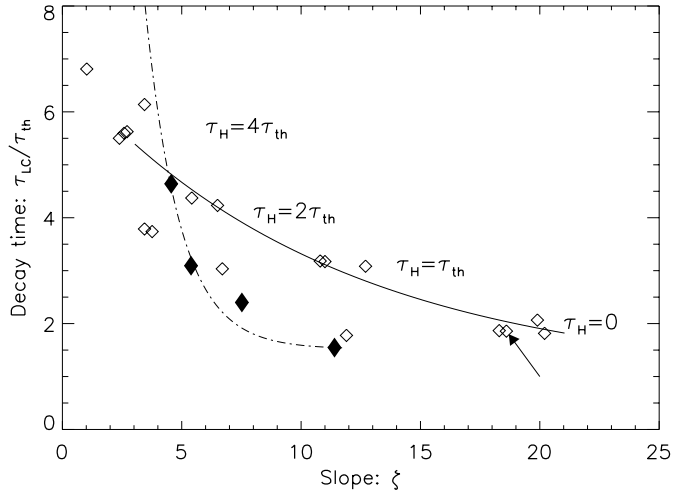


**Fig. 3.** Decay time of synthesized PSPC light curves vs. slope $\zeta$ in the CR2-SSI diagram (as of Fig. 2) for 22 model loops, of which 18 have length smaller than (*empty diamonds*), and 4 comparable to (*filled diamonds*), the pressure scale height (see text for details), with various values of the heating e-folding time $\tau_H$. The *arrow* points to the model shown in Fig. 2. We also show the functions (5) (*solid*) and (7) (*dotted-dashed*) which we use to fit the model results.

the slope $\zeta$ in the CR2-SSI diagram for all solar models in Paper I, plus others computed to extend the study to other stars, with different gravity ($g$) and radius ($R$). As illustrated by Reale et al. (1993), the application to other stars involves no new model classification, except that we have to distinguish between flaring loops that are longer and shorter than the local pressure scale height. In this study we consider the nine models presented in Paper I, with solar gravity and radius (loop half-length $L = 2\times10^9$ cm and $L = 10^{10}$ cm) and heating decay times $\tau_H = 0, 1, 2, 4\tau_{th}$; $T_{max} = 2\times10^7$ K for all the models but one, $T_{max} = 3\times10^7$ K ($L = 2\times10^9$ cm, $\tau_H = 0$). We add a further solar model with $L = 2\times10^9$ cm, $T_{max} = 2\times10^7$ K and $\tau_H = 6\tau_{th}$. The additional "stellar" models include decaying loops much shorter than the pressure scale height for other two values of gravity, one lower ($g = 0.1g_\odot$) and one higher ($g = 3g_\odot$) than the solar gravity. We assume $R = R_\odot$ and $R = 0.3R_\odot$, respectively. The half-length and the maximum temperature of all these loops are $L = 2\times10^9$ cm and $T_{max} = 2\times10^7$ K, respectively. For each value of $g$ we consider models for four values of $\tau_H$ ($0, 1, 2, 4\tau_{th}$).

As for long loops, we include four loop models with half-length comparable to pressure scale height $L/s_h \sim 1$, with high gravity $g = 10g_\odot$, small radius $R = 0.15R_\odot$, loop half-length $10^{10}$ cm, temperature $T_{max} = 1.5\times10^7$ K, and the four heating decay times ($\tau_H = 0, 1, 2, 4\tau_{th}$).

We come out with a total of 22 model flaring loops, of which 18 are loops smaller than the pressure scale height.

As shown by Fig. 3, for the loops shorter than the pressure scale height ($g \le 3g_\odot$), we find the same general trend as found in Paper I for Yohkoh/SXT: models with $\tau_H = 0$ are grouped on the low right-hand side, while the slope $\zeta$ of the others ($\tau_H \neq 0$) decreases and the ratio $\tau_{LC}/\tau_{th}$ increases as the heating time increases.

We notice that the range spanned by $\zeta$ ($0 \lesssim \zeta \lesssim 20$) in the CR2-SSI diagram is much larger than in the n-T diagram (see Paper I). As done in Paper I, we fit the short loop model points in this plane with a given functional form. Although the trend looks similar to that found in Paper I, the different distribution of the models, and in particular the more rapid and regular decrease of $\zeta$ with increasing $\tau_{LC}/\tau_{th}$, makes it difficult and inappropriate to fit the results with hyperbolic functional forms, as we did in Paper I. We have therefore chosen to fit them with decaying exponentials. In this case, we cannot impose an asymptotic behaviour for low $\zeta$, and we choose $\zeta = 3$ as a lower limit of the validity of our fitting, a value safely larger than $\zeta \sim 2$ expected for the slope of the trajectory traced by the hydrostatic loop models (the QSS curve, see Jakimiec et al. 1992). The fitting function for short loops is therefore:

$$\tau_{LC}/\tau_{th} = c_a \exp(-\zeta/\zeta_a) + q_a = F_a(\zeta) \qquad (5)$$

with:

$$c_a = 5.85 \pm 0.02 \quad \zeta_a = 10.9 \pm 0.4 \quad q_a = 0.94 \pm 0.01$$

where $c_a$, $\zeta_a$ and $q_a$ have been found with a linear regression on $\ln(\tau_{LC}/\tau_{th})$ on all models with $L = 2\times10^9$ cm.

From Eq. (1) and Eq. (5) we derive the expression for $L$:

$$L_a = \frac{\tau_{LC}\sqrt{T_{max}}}{\alpha F_a(\zeta)} \qquad 3 \lesssim \zeta \lesssim 20 \qquad (6)$$

Values larger than $\zeta \approx 20$ should not be allowed according to our modelling.

Let's now turn our attention to the model loops with length comparable to the pressure scale height. Despite a different and more general $\tau_{th}$ has been defined in Reale et al. (1993), we will still use the one defined in Serio et al. (1991) even for these long loops, i.e. we are considering the decay time in the very initial phases of the decay, when the effect of gravity is not important. As expected (Reale et al. 1993), for small $\tau_H$ these models lie in a region separate from shorter loops: lower and leftwards in Fig. 3, i.e. the decay of the light curves is faster, and, as shown in Reale et al. (1993), the slope $\zeta$ in the n-T diagram is smaller, the maximum being $\zeta \approx 12$ when $\tau_H = 0$. Both effects are due to the higher effect of gravity: the plasma precipitates downwards more rapidly, and its density decreases faster along the loop, while affecting less the temperature decay.

We use the functional form (5) and extend the expression (6) also to loops comparable to the pressure scale height, with different numerical parameters:

$$\tau_{LC}/\tau_{th} = c_A \exp(-\zeta/\zeta_A) + q_A = F_A(\zeta) \qquad (7)$$

with

$$c_A = 70.9 \pm 0.4 \quad \zeta_A = 1.45 \pm 0.15 \quad q_A = 1.52 \pm 0.01$$

$$L_A = \frac{\tau_{LC}\sqrt{T_{max}}}{\alpha F_A(\zeta)} \qquad 4 \lesssim \zeta \lesssim 12 \qquad (8)$$

Eq. (7) fits the four models as shown by Fig. 3. Notice that a smaller $\zeta$ range is permitted for such long loops.

The crossing of two curves shown in Fig. 3 at $\zeta \sim 4$ is consistent with the fact that the QSS model slope in the CR2-SSI diagram for models longer than the pressure scale height is larger ($\zeta \approx 4$) than for shorter loops ($\zeta \approx 2$). This intersection has no consequence in the determination of the loop length, because the related formulae are independent of each other. It is worth noting that values $\zeta < 4$ are forbidden for very large loops and should be a signature of loops shorter than $s_h$.

We end up with two different expressions for $L$, one valid for loops shorter than the pressure scale height ($L_a$), the other for longer loops ($L_A$). The problem now arises, which one to use, when we analyze real stellar data with $4 \lesssim \zeta \lesssim 12$, and do not know (of course) the loop length *a priori*, as we do for models. The problem is only apparent, because we have to obtain a self-consistent result: if we apply expression (6) then the resulting loop must be shorter than the pressure scale height, otherwise we have to use expression (8) ($L/s_h \gtrsim 0.5$).

Notice finally that, once given the flare light curve and temperature, there is a limited range of possible loop lengths, since $1.9 \lesssim F_a \lesssim 5.4$ and $1.5 \lesssim F_A \lesssim 6$. In particular, if only $\tau_{LC}$ and $T_{max}$are known we obtain upper limits for the flaring loop length given by the lowest values of $F_{a,A}$.

### *2.4. Accuracy and limitations*

As remarked in Paper I, this procedure to determine the length of stellar flaring loops is subject to some restrictions and limitations. As for model assumptions, although often too simplistic for real flaring structures, they have been proven to be adequate for the description of global and average quantities of solar flares (Paper I).

Outside model assumptions, there are essentially two conceptually different sources of uncertainty in the loop length determination of Eqs. (6) and (8): i) the scattering of the model points in Fig. 3 and the assumption of the empirical functional form (Eqs. 5 and 7); ii) the data statistics, which affects the accuracy of the light curve decay time, the count rate and SSI values, and the slope in the CR2-SSI plane.

In order to quantify the first source of uncertainty, but also to check whether the procedure provides self-consistent results on the model loops themselves, we have applied Eqs. (6) and (8) to the model loops, deriving $T_{max}$from the relationship shown in Fig. 1. We remark that for loops longer than the pressure scale height, the method is calibrated on the temperature *at* the pressure scale height (not at the loop apex).

Fig. 4 shows the distribution of the deviations of the predicted from the true length values $\log(L_{pred}/L_{true})$ for the 22 models in Fig. 3. The distribution of $L_{pred}/L_{true}$ is quite well centered around the zero value (median +0.4%), i.e. systematic effects are small, and the standard deviation is 19%, which may be taken as an estimate of the uncertainty associated purely with the modeling. We have ascertained that such deviation is independent of $\zeta$.

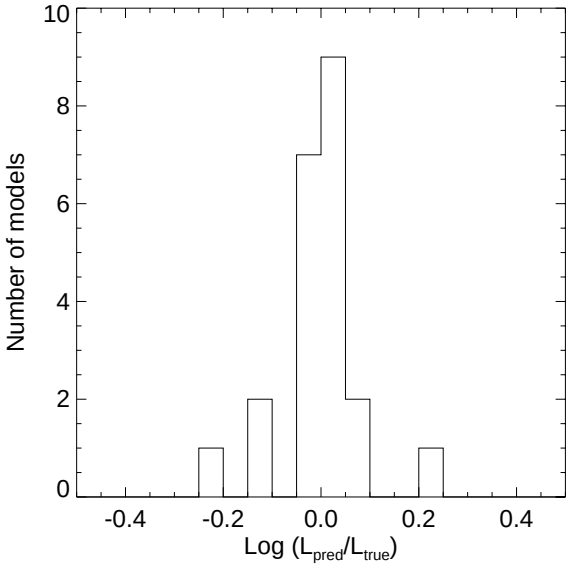


**Fig. 4.** Distribution of $\log(L_{pred})/L_{true})$ (ratio of the predicted and real loop lengths) for the models in Fig. 3, where $L_{pred}$ is obtained using Eqs. (6) and (8).

In order to estimate the uncertainty due to data statistics, we have performed several simulations of real data and studied the distribution of the resulting loop lengths. We have selected several hydrodynamic models of decaying loops and, for each one, all the spectra between the maximum and 1/3 of the maximum of the light curve, a realistic range for typical flare observations. We have grouped these spectra into four time bins of such duration as to yield approximately the same total counts. Then we have fixed a data statistics (the total number of counts for each bin), and we have applied a bootstrapping procedure to each spectrum. For each decay model we therefore obtain several groups of four spectra with approximately the same total counts, which we analyze exactly as if they were real data, by deriving the light curve decay time and the slope in the CR2-SSI diagram, and, from them, the expected loop length. Our error estimate on $L$ will be the standard deviation of the loop length values.

We have considered the models with $L = 2 \times 10^9$ cm, maximum temperature $T_{max} = 2 \times 10^7$ K, and three heating decay times ($\tau_H = 0, 1, 2\tau_{th}$). For each model we have selected seven count statistics (from 100 to 10000 counts per bin) and made one thousand simulations for each selection. In Table 2 we show, for the selected values of data statistics, the typical standard deviations of some relevant quantities, as obtained from the simulations. For each data statistics we report a single value of the deviations, since they depend little on the model (they slightly increase with $\tau_H$, with variations within $\sim 10\%$). The table shows the mean standard deviation $\Delta SSI$ (column 2) of each value of SSI (which depends little on the value of SSI), of the slopes $\Delta\zeta$ (column 3), and, fractional, of the decay time $\Delta\tau_{LC}/\tau_{LC}$ (column 4), of the predicted loop length $(\Delta L/L)_{stat}$ (column 5). The last column (6) contains the total estimated uncertainty in the predicted length, which

**Table 2.** Mean error estimates for the flare decay analysis

| counts | $\Delta$ SSI | $\Delta\zeta$ | $\Delta\tau_{LC}/\tau_{LC}$ | $(\Delta L/L)_{stat}$ | $(\Delta L/L)_{tot}$ |
|---|---|---|---|---|---|
| (1) | (2) | (3) | (4) | (5) | (6) |
| 100 | 1.5 | 10 | 0.09 | $> 1$ | $> 1$ |
| 300 | 0.9 | 6 | 0.07 | 0.7 | 0.7 |
| 500 | 0.7 | 5 | 0.05 | 0.6 | 0.6 |
| 1000 | 0.5 | 3 | 0.04 | 0.4 | 0.4 |
| 3000 | 0.3 | 2 | 0.02 | 0.24 | 0.3 |
| 5000 | 0.2 | 1.5 | 0.02 | 0.18 | 0.3 |
| 10000 | 0.15 | 1.2 | 0.01 | 0.13 | 0.2 |

is obtained by summing in quadrature the deviation obtained from the simulations ($(\Delta L/L)_{stat}$) to that obtained from pure modeling (19%).

All the standard deviations decrease with the number of counts, as may be expected. With 10000 counts per bin the total uncertainty in the length is only 20%, with 1000 it is still about 40%. Even with 300-500 counts per bin one may expect to obtain useful information from the analysis. For 100 counts per bin the predicted length is practically undetermined.

### *2.5. Effect of absorption*

X-ray spectra of distant stars, or of stars enclosed in interstellar clouds, are distorted by the absorption by interstellar gas. We now discuss its influence on our diagnostics and in particular on Eqs. (6) and (8).

Significant effects on the results are to be expected because the soft parts of the spectra are absorbed more than the hard parts. This means that the value of the SSI, as well as the total count rate, of an absorbed spectrum will, in general, be different from that of the same non-absorbed spectrum; therefore, in general, also the slope $\zeta$ will no longer be the same.

In order to investigate this effect, we have applied an absorption model with parameters from Morrison & McCammon (1983) to all spectra synthesized from the hydrodynamic simulations, with various values of the hydrogen column density.

We have verified that: i) absorption produces no significant effect for $\log N_H \lesssim 19$; ii) for $\log N_H \sim 20$ the values of $\zeta$ are substantially unchanged, thus Eqs. (6) and (8) still hold (median +5%, standard deviation 19% in the self-consistency test), but the flare temperature at the loop apex should be estimated using the thin lines in Fig. 1; iii) for $\log N_H \sim 21$ the SSI no longer provides a good representation and Eq. (6-8) are no longer applicable; however we have devised a way to apply them again even to such absorbed spectra (median +1%, standard deviation 26%) by converting their SSI to "non-absorbed" values using the relationship shown in Fig. 5, approximately valid both for short and long loops. This relationship has been derived by using the hydrostatic loop models mentioned above.

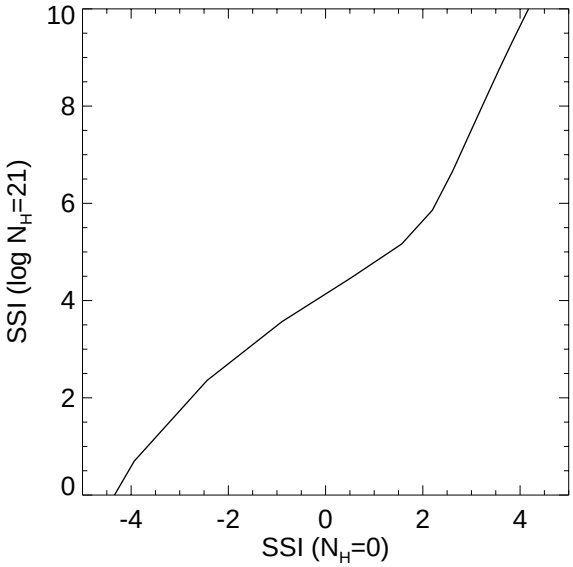


**Fig. 5.** Spectral shape index (SSI) of hydrostatic models of loops (shorter than the pressure scale height, see Fig. 1) absorbed by a hydrogen column $\log N_H = 21$ vs. SSI of the same non-absorbed spectra.

## 3. Applications

### *3.1. A flare on AD Leo*

We have applied the technique described above to a flare observed on the dM3.5e star AD Leo (distance 4.9 pc, radius 0.4 $R_\odot$, gravity $\log g = 4.7$, from Allen 1976). AD Leo has been observed in the pointing 200076 from 8 to 9 May 1991 for a total exposure time of 26522 sec (Giampapa et al. 1996). In this exposure the star is highly variable and includes at least two flares.

We have divided the flare decay phase into four segments of the same duration ($\approx 150$ sec), starting from 48384.6 MJD. Then we have considered the four spectra as integrated in each segment, by subtracting from them the average quiescent spectrum as observed in the period before the flare. The four resulting ROSAT spectra contain 723, 573, 462 and 335 counts, respectively, in the 28 channels of interest. The average number of counts per bin is 523. The effect of the absorption is negligible for this star. The count rate decreases approximately by a factor of two from the beginning of the decay to the end of the data.

We now apply Eqs. (6) and (8). As shown in Fig. 6, both the light curve and the trajectory in the CR2-SSI diagram are well-defined and monotonic. The maximum SSI value $SSI_{max} \approx 4$ corresponds to a temperature at the loop apex $T_{max} \approx 35$ MK (see Fig. 1). The slope in the CR2-SSI diagram is $\zeta \approx 14$ which falls in the region of moderate heating times ($0 \lesssim \tau_H \lesssim \tau_{th}$) (Fig. 3). From Eqs. (6) and (8) we obtain a loop half-length value $L \approx 4\ 10^9$ cm, with an uncertainty $\sim 60\%$ (see Table 2). This loop half-length value is $\sim 1/7$ of the stellar radius, i.e. a proportionally large flaring loop with respect to solar flaring loops in active regions, which, however, may not be unusual on M stars (see Reale et al. 1988). This length is still well below the pressure scale height. The value we would obtain from Eq. (1),

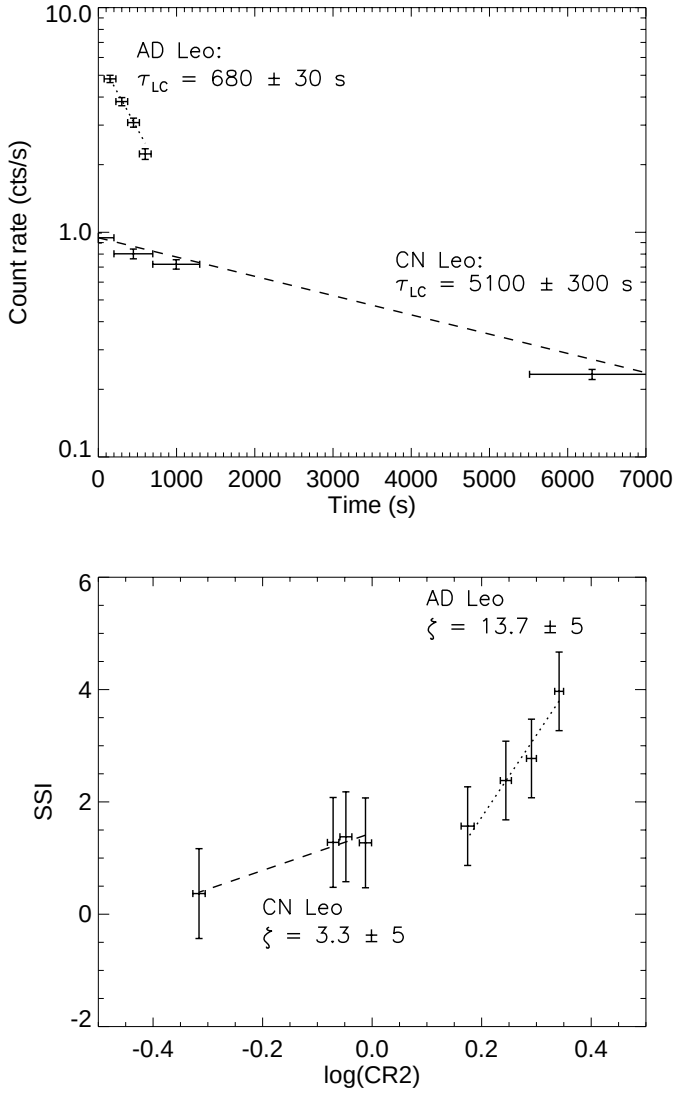


**Fig. 6.** ROSAT/PSPC light curve (*upper panel*) and trajectory in the $CR2-SSI$ diagram (*lower panel*) of the decay of two flares observed on the dMe stars AD Leo and CN Leo. The horizontal error bars mark the duration of each time bin. The decay lines (*dashed*) and their slopes ($\tau_{LC}$ and $\zeta$) are shown.

by posing $\tau_{LC} = \tau_{th}$, is $L \approx 10^{10}$ cm, more than twice the value that we obtain, although this is a case of moderate heating during the decay. In turn this length is shorter than what we would obtain from combinations of radiative and conductive cooling times, as generally used by many authors to estimate stellar flaring loop lengths (see Paper I).

In summary, we come out with a scenario of a flare in a relatively large loop, but shorter than expected solely from plasma cooling times, and a relatively small heating during the decay ($\tau_H < 300$ sec).

### *3.2. A flare on CN Leo*

We have applied our method to a second flare observed by the PSPC on CN Leo (GJ 406), a M6 star at the distance of 2.39 pc belonging to the old disk population. It has been pointed for a total observing time of 4.2 ksec in two observations (pointings 201577 and 201722) on 4-5 December 1993, which span a time interval of 14 ksec, and which have been subdivided in three data segments. We have analyzed the decay phase as starting from the beginning of the observation and including the first two data segments. The count rate during the observed flare decay decreases by about a factor four. We have divided the first data segment in three time bins of 400, 500, and 593 sec, respectively, while the second data segment has been analyzed in its entirety (1606 sec). We have subtracted the spectrum measured in the quiescent phase (that we assume to be observed in the third data segment) from the spectra measured in each time bin, thus obtaining for the four bins 378, 398, 432 and 373 counts, respectively, with an average of $\approx 400$ counts.

We now apply Eqs. (6) and (8), as we did for the flare on AD Leo. As shown in Fig. 6, the light curve decay is slower (more than an hour) than for the previous flare, suggesting a larger structure, while the slope $\zeta$ is considerably smaller (close to the lower limit $\zeta = 3$), which indicates a significant sustained heating ($\tau_H \gtrsim 2\tau_{th}$). The maximum temperature is estimated to be about 7.5 MK ($SSI_{max} \approx 1.3$). The expected loop half-length is $L \approx 7\ 10^9$ cm (with an uncertainty between 60% and 70%), which, if we assume a gravity $2.3 g_\odot$ and a radius $0.3 R_\odot$ of a dM5 star (Allen 1976), is still well below the pressure scale height and smaller than the stellar radius. Notice that the central slope value is smaller than 4, thus implying a flaring loop smaller than the pressure scale height. Notice also that, even considering the error bars, the slope indicates unequivocally the presence of significant heating during the decay. From Eq. (1), by posing $\tau_{LC} = \tau_{th}$, we would obtain $L \approx 4 \times 10^{10}$ cm, larger than the pressure scale height and even than the stellar radius, suggesting an unrealistically large structure. A self-consistent scenario for the flaring loop is, in summary, quite a large structure, but still well within the limit of realistic coronal loops.

## 4. Summary and conclusions

We have described a procedure to derive the length of coronal loops from the analysis of the flare decay of stellar flares observed with ROSAT/PSPC. Although the method presented here is tailored to ROSAT/PSPC flare observations, the approach is general for any X-ray observation with at least moderate spectral resolution.

The major achievements of our approach are to include the effect of sustained heating during the decay and to properly take into account the instrumental spectral response in the analysis of the light curve, thanks to the use of numerical modeling.

We take full advantage of PSPC data by using a model-independent spectral shape index (SSI), which allows us to bypass the step of model-dependent temperature fitting. This enables us to improve sensitivity to the thermal decay of stellar flares, whereas standard temperature analysis provides no information.

Although we make extensive use of numerical hydrodynamic modeling, the final results of our approach are two ex-

pressions for the loop length, one for short and the other for long loops compared to the pressure scale height, for which only the light curve decay time, the maximum flare temperature and the slope of the decay in the CR2-SSI diagram need to be known (see Sect. 2). No detailed modeling of each observed flare is required. The formulae provide upper limits on the loop length if no spectral information is available, as shown at the end of Sect. 2.3.

The self-consistency tests conducted on the models indicate that no significant systematic errors arise from the application of the formulae. With the aid of data simulations, we have also provided detailed estimates of the uncertainties of the length prediction, which show that useful indications can be drawn from flare decays yielding more than $\sim 1000$ counts in total.

The application to two specific PSPC flares on two M stars has shown the potentiality of the length prediction. We are able to constrain the structure dimensions, to state whether there is significant heating or not, and to provide possible values for the heating decay time. In the case of the flare observed on CN Leo we obtain a length value considerably smaller than the expected stellar radius, whereas estimates simply based on plasma cooling times suggest structures well beyond the radius, thus calling for *ad hoc* morphological explanations.

The method is very appropriate for extensive and systematic application to flare surveys observed with ROSAT/PSPC, although in the limit of the applicability and of the indeterminations due to modeling and to data statistics. It should allow us to study statistically the distribution of the dimensions of stellar flaring loops, crucial to understand stellar coronal physics. Furthermore, the identification of significant heating during the decay and the estimation of the heating decay time, in connection with the different stellar environment conditions, will certainly make it possible to investigate the flare heating mechanisms under a new perspective.

Analogous expressions for the loop length can be easily extracted for other X-ray instruments such as *Einstein*/IPC, ASCA/SIS, or forth-coming ones, such as on AXAF and XMM.

*Acknowledgements.* We thank R. Betta and S. Sciortino for collaboration in the hydrodynamic numerical modeling and in the data analysis, respectively, S. Serio, G. Peres and D. Randazzo for suggestions. We acknowledge partial support from Ministero dell'Università e della Ricerca Scientifica e Tecnologica, Agenzia Spaziale Italiana and Consiglio Nazionale delle Ricerche.

## References

Allen C. W., 1976, Astrophysical Quantities, Athlone Press (London).
Betta R. M., Peres G., Serio S., Reale F., 1997, A&AS 122, 585.
Ciaravella A., Maggio A., Peres G., 1997, A&A in press.
Collura A., Micela G., Sciortino S., Harnden F. R. Jr., Rosner R. 1995, ApJ 446, 108
Giacconi R., Branduardi G., Briel U., et al. 1979, ApJ 230, 540.
Giampapa M. S., Rosner R., Kashyap V., et al., 1996, ApJ 463, 707.
Haisch B.M., 1983, in Activity in Red-Dwarf Stars, eds. P.B. Byrne, M. Rodonó, Reidel, Dordrecht, p.255.
Haisch B.M., Strong K. T., Rodonò M., 1991, ARA&A 29,275.
Jakimiec J., Sylwester B., Sylwester J., et al., 1992, A&A 253, 269.
Maggio A., Peres G., 1996, A&A 306, 563.
Morrison R., McCammon D., 1983, ApJ 270, 119.
Murtagh F., Heck A. 1987, Multivariate Data Analysis (Boston: Reidel Publishing Company).
Raymond J. C., Smith B. W., 1977, ApJS 35, 419.
Reale F., Peres G., Serio S., Rosner R., Schmitt J.H.M.M., 1988, ApJ 328, 256.
Reale F., Serio S., Peres G., 1993, A&A 272, 486.
Reale F., Betta R., Peres G., Serio S., McTiernan J., 1997, A&A 325, 782 (paper I)
Sciortino S., Micela G., Reale F., et al., 1996, Magnetohydrodynamic Phenomena in the Solar Atmosphere - Prototypes of Stellar Magnetic Activity, Y. Uchida et al. (eds.), Kluwer Academic Publishers (Dordrecht), 277.
Serio S., Peres G., Vaiana G. S., Golub L., Rosner R., 1981, ApJ 243, 288.
Serio S., Reale F., Jakimiec J., Sylwester B., Sylwester J., 1991, A&A 241, 197.
van den Oord G.H.J., Mewe R., Brinkman A.C., 1988, A&A 205, 181.